NUMERICAL SIMULATION ANALYSIS OF NEW MELTING STRATEGIES FOR THE POWDER BED FUSION WITH ELECTRON BEAM

PEDRO HERNANZ
POLITECNICO DI TORINO

Table of Contents

INTRODUCTION

Throughout history, traditional manufacturing has been practiced, which consisted of producing objects through processes that commonly involved removing material until the desired shape of the object to be manufactured was achieved. However, with the advancement of technology, strategies known as additive manufacturing have been developed, which involve creating objects by adding material, contrary to what had been done in the past.

There are numerous types of additive manufacturing depending on various factors, such as the material used, the technology employed, etc.

One of the existing technologies is called EBM (Electron Beam Melting). In broad terms, this consists of using an electron beam that acts on a powder material, this beam fuses the powder it hits, transforming it into a solid form, generating objects by performing multiple passes layer by layer.

The most widespread strategy for melting the material is called “hatching”, this method melts the powder area of the material using linear patterns, thereby filling in its contour (1). Although this strategy achieves generally acceptable final results, it presents certain limitations such as the presence of rough surfaces, difficulty in cases with complex surfaces, and challenges in controlling temperature in specific zones, which results in some points of the material not being fully melted (2).

Due to these limitations, different strategies have been continuously developed to improve the EBM process. Among them is the “point melt” strategy, which consists of melting the powder by means of individual spots rather than the continuous lines used in hatching. This way, it is possible to achieve high precision in obtaining the desired shape and great control of the temperature, ensuring that all the intended material is melted.

The problem with this strategy is that, since it is still being researched, it has not yet been sufficiently developed to achieve a higher efficiency (3).

The main objective of this work will be to analyze, through a numerical simulation by finite elements performed in the ABAQUS program, how modifying certain beam parameters affects the EBM process using the point melt strategy, seeking the most optimal combination of parameters so that our manufacturing process is as reliable and efficient as possible.

The structure of the work will consist first of doing a study of all the necessary theory to contextualize the process to be studied, then showing the procedure of how the model used for our simulations was built, and finally, analyzing the results obtained in these simulations.

LITERATURE REVIEW

ADDITIVE MANUFACTURING

Additive manufacturing is a revolutionary manufacturing process that has been implemented and improved since the late 20th century.

It can be defined as the process of joining materials with the aim of forming objects from a 3D model. This joining is usually performed layer by layer, in contrast to traditional manufacturing processes, which are typically based on subtractive manufacturing, that is creating the desired object by removing material from a block with a simpler geometry (4).

This type of manufacturing is extremely practical when dealing with low production volumes, parts that are involved in numerous design changes over time, and when there is a need to manufacture parts with high design complexity.

When comparing additive manufacturing to traditional manufacturing, several notable advantages stand out. Among the most important we find the adaptability it offers, because in a traditional manufacturing process, a part may be required to go through several of different operations, each performed on machines specialized for a single process, but with additive manufacturing this is not the case, as it is possible to produce parts with great complexity in shape using just one machine and one process.

This adaptability makes additive manufacturing very useful in contexts such as the aerospace and defense industries, where countless types of parts can be produced in a small space, eliminating the need for spare parts and providing significant savings in storage.

Another industry where its potential is evident is the medical field, as it allows the production of fully customized parts for each patient. This makes possible to create prostheses that perfectly fit the anatomy of each individual at a much lower cost than traditional manufacturing.

This information is relevant because this work uses a metal, specifically Ti6Al4V, which will be discussed further later.

Finally, it is important to consider the materials used in this type of technology, which can be seen in the following chart Fig. 1, this figure shows the distribution of the use of the different types of materials used in additive manufacturing processes.

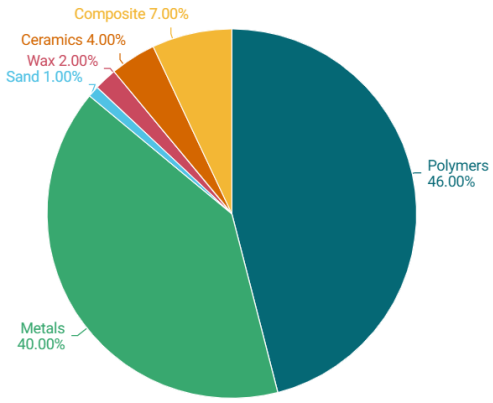

Fig. 1: Types of material in additive manufacturing (4).

It can be observed that the most common materials are polymers and metals, followed by others with less prevalence such as sands, waxes, ceramics, and composites.

EBM

With an understanding of what additive manufacturing is about, it should be understanded that there are many ways to employ this technology when working with metals.

There are four main ways to classify metal additive manufacturing depending on the type of technology being used, as shown in Fig. 2.

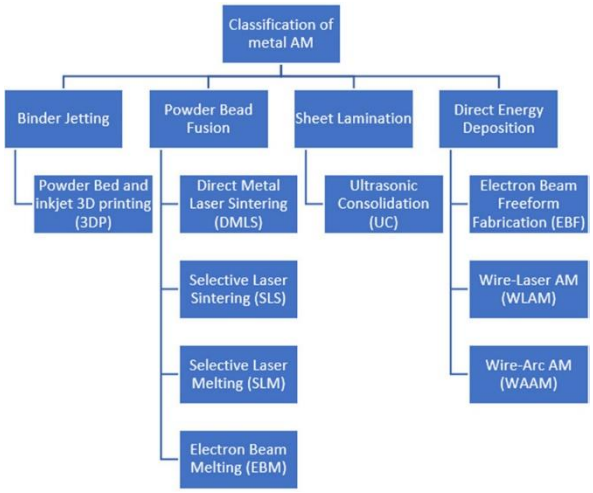

Fig. 2: Classification of metal additive manufacturing technologies. (19)

In this case study, powder-based additive manufacturing using a powder bed with full fusion consolidation, carried out with the help of an electron beam is employed. This technology is known as EBM (Electron Beam Melting).

EBM is one of the only processes that are capable of making full-density functional parts, especially complex parts made of excellent quality material (5).

This process operates in a vacuum atmosphere, which allows it to work safely at temperatures above 870 (ºKelvin). Working at such high temperatures also involves longer cooling processes compared to other similar methods (6).

It is worth noting that in this type of process, more parameters come are relevant compared to those involved in similar processes. The most notable are (6):

- Beam power
- Beam scan speed
- Beam focus
- Beam diameter
- Beam line spacing
- Plate temperature

- Preheating temperature
- Contour strategies
- Scanning strategy

To fully understand the EBM process, the main steps performed in a typical process are listed below (5).

1. **Generation of the electron beam**
    - Electrons are extracted from a tungsten filament in a vacuum chamber; they are accelerated and focused by electromagnetic fields to form a concentrated beam.
2. **Preparation of the start plate**
    - Heat of the base plate to a temperature defined according to the powder material to be melted (7), this temperature is controlled by the power of the electron beam.
3. **Deposition of the first powder layer**
    - A thin and uniform layer of metal powder is spread over the start plate.
4. **Preheating of the powder bed**
    - This is done by defocused passes of the beam at high power and high speed, which helps to avoid thermal stresses and improve adhesion between layers.
5. **Selective melting of the powder particles**
    - The electron beam selectively melts the powder according to the CAD design, forming the first solid layer or a support structure.
6. **Cooling of the part**
    - The part cools slowly under a helium atmosphere at increased pressure to prevent oxidation.
7. **Lowering of the platform**
    - The build platform descends by one layer thickness.
8. **Spreading of a new powder layer**
    - A new layer of powder is distributed over the previous one.

9. **Repetition of the melting process**

    - The electron beam melts the new layer according to the desired pattern. This cycle is repeated layer by layer until the part is completed.

10. **Part removal and cleaning**

    - Upon removal, a soft agglomerated powder called “breakaway powder” (8) remains adhered, this powder is removed by sandblasting using the same powder used during the process (9).

11. **Recycling of unused powder**

    - Unmelted powder can be recycled several times without altering its chemical composition or physical properties, provided that minimal oxygen absorption has not occurred inside the chamber during the melting process (5).

To understand the process in a simplified way, the schematic in Fig. 3 is shown.

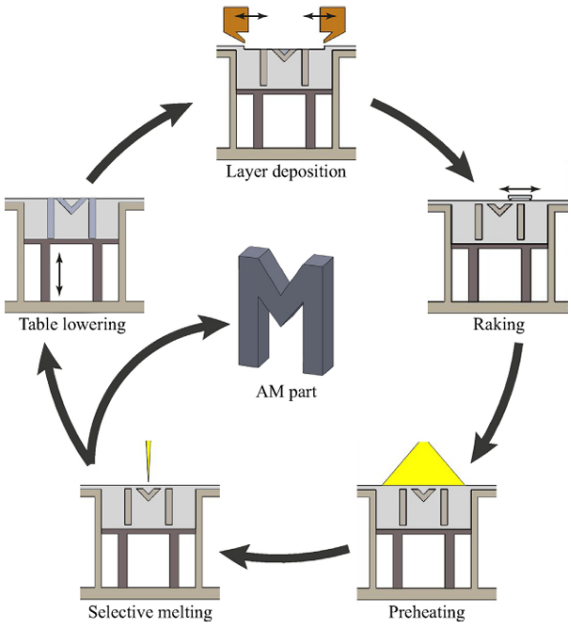

Fig. 3: The phases of the EBM process (5)

HARDWARE OF A EBM MACHINE

Having understood the step-by-step operation of the EBM manufacturing process, the study proceeds to analyze a machine capable of performing this type of process.

The machine studied is shown in Fig. 4, it is the ARCAM A2 system. This system has been designed for aerospace and defense industry applications since the build chamber can be interchanged to accommodate either wide or tall components (10).

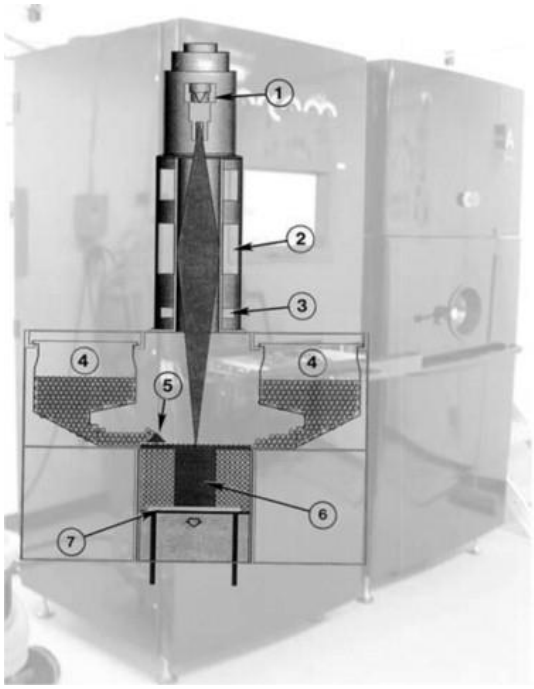

Fig. 4: ARCAM A2 system (10)

Study of the components in Fig. 4:

1. **Electron gun**
    - Tungsten filament operating with a current of approximately 10 (A) and an anode potential of 60 (kV).
2. **Electromagnetic lenses**
    - Used to focus the electron beam.
3. **Scanning coils**
    - Control the movement of the electron beam in the X and Y directions with scan speeds up to 1000(mm/s) and an accuracy of ±0.025(mm).

4. **Powder tanks**
    - Located on each side of the machine, their purpose is to feed the build platform with metal powder by gravity.
5. **Rake**
    - Responsible for evenly distributing the powder over the build platform in thin layers.
6. **Building chamber**
    - The area where melting and solidification occur to create the solid part.
7. **Building table**
    - Moves downward after each pass to allow the sequential construction of the part.

POINTMELT

Within EBM itself, it is possible to work with different strategies depending on the desired application of the beam. Normally, strategies called "hatching" are used, in which our metal powders are fused following continuous paths.

Despite this, and in the pursuit of optimizing processes, promising alternatives to continuous paths in the EBM process are being developed. One of these alternatives consists in create discontinuous heating trajectories by jumping to specific positions, this is referred to as the the "point melt" strategy. In contrast to the sequential nature of hatching patterns, the feasibility of the point melt strategy is made possible by the high translation speed of the electron beam. This feature allows the beam to move almost instantaneously between different positions, activating multiple melt pools at various locations within the cross-sectional area of the design (11).

In our study, this point melt strategy will be used because it allows more precise temperature control, reducing thermal gradients, the need for sintering, and ensuring a better surface finish (12).

MODELLING

In order to avoid experimental trial-and-error processes to find the ideal parameters when working with EBM, various models have been developed over recent years to simulate EBM conditions (13). However, all of them present issues in one way or another, either because they do not consider certain important parameters or due to their high cost caused by excessive complexity.

We must keep in mind that EBM simulation models need to consider three fundamental aspects (13):

- An adequate analytical model of the material properties.
- Modelling of the thermal energy source.
- A numerical implementation to solve the complexity of the phenomena, considering the above aspects.

For this study, the model developed by Galati, Iuliano, Salmi and Atzeni is utilized (13). This model implements a new type of modelling for both the energy source and the powder material with the goal of improving the efficiency and reliability of finite element simulation by developing subroutines for the following scenarios:

1. Automatically calculating the powder properties as a function of temperature.
2. Considering the position of the beam during scanning.
3. Simulating phase changes of the material (from powder to liquid during melting, and from liquid to solid during cooling).

In (13), experiments confirm that the average deviations of the simulation compared to experimental tests are less than 15%, making it a highly reliable simulation model that fits our requirements.

ENERGY SOURCE

The modelling of our energy source is based on Monte Carlo simulations of the moment when the electron beam impacts the material, estimating the trajectories of the electrons in a sample. The most important factors to consider in this simulation are (13):

- Material density.
- Alloy elements and their atomic numbers.
- Energy or acceleration voltage of the beam.
- Diameter of the focused beam.

Based on this simulation, the heat source is modelled as a uniform distribution applied over a surface equivalent to the cross-sectional area of the electron beam.

The heat flux intensity, hereafter referred to as "q" and expressed in (W/mm^2), will be determined using the Equation 1:

$$\mathbf{q} = \eta \frac{UI}{S}$$

Equation 1: Equation for heat flux intensity (13)

Where:

- **U**: Acceleration voltage (kV)
- **I**: Beam current (mA)
- **S = (π D^2) / 4**: Cross-sectional area of the beam (mm^2)
- ***η*:** Correction coefficient

For the calculation of the correction coefficient η, Equation 2 is used:

$$\eta = \int_{\Gamma} \frac{1}{2\pi\sigma^2} \exp\left(-\frac{(x_1 - x_{10})^2 - (x_2 - x_{20})^2}{2\sigma^2}\right)$$

Equation 2: Equation for correction coefficient (13)

Where:

- **Γ:** Cross-sectional area of the beam.
- **x1 and x2:** Generic Cartesian coordinates.
- **x10 and x20:** Coordinates of the initial point of the center of the electron beam focus.
- **σ:** Standard deviation of the effective beam diameter "DE," which represents the lateral dispersion of electrons upon impacting the powder layer. This value is obtained from Monte Carlo simulations and depends on the material and its density, the acceleration voltage, the actual beam diameter, and the beam current.

  The calculation of this deviation will be performed as follows in Equation 3:

$$\sigma = D_E/4$$

Equation 3: Equation for the standard deviation (13)

The Fig. 5 shows an example of simulations performed with the electron beam interacting with a layer of Ti6Al4V.

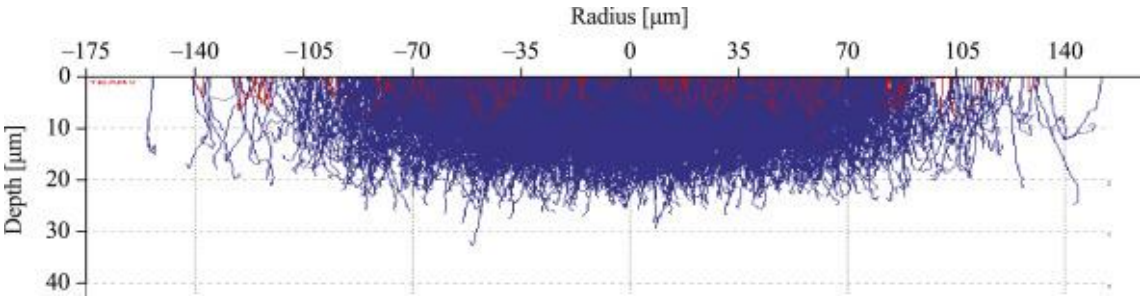

Fig. 5: Electron trajectories in a cross-section of a Ti6Al4V sample. The electron trajectory simulation has been performed with the CASINO software. The red lines refer to back-scattered electron trajectories, while the blue lines refer to the paths of non-back-scattered electrons. An acceleration voltage of 60 kV and a beam diameter of 0.272 mm have been used. (14)

To implement this beam simulation in ABAQUS, a DFLUX subroutine will be used, which allows us to define heat flux dependent on position and time (13), based on all the parameters defined in each simulation, such as the time when the beam starts and stops operating, its diameter, its power, and the material properties. In this work, a static process will be considered, so the beam will be applied at a fixed location and no accounting for its movement is necessary.

HEAT TRANSFER

To define how this heat transfer will thermally affect our material in the model, it must be understanded that heat transfer occurs through three different mechanisms (13):

- Heat conduction between powder particles.
- Heat conduction between the powder bed and the solid substrate.
- Radiation from the powder bed to the chamber.

To simplify the analysis, it will be only considered these mechanisms in our model.

In this model, the substrate and the solid are modelled as a continuum, so the fundamental laws of (13), can be applied, which consider:

- Conservation of mass.
- Conservation of momentum.
- Conservation of energy.

These lead to differential equations that describe the thermal behaviour during the process.

Considering energy conservation, the absolute temperature distribution is defined as T(x1,x2,x3) within a homogeneous body where there is no matter exchange, expressed in Cartesian coordinates. The energy balance per unit volume inside an infinitesimal control volume of dimensions dx1,dx2,dx3 at a given instant in time can be expressed in differential form as in Equation 4:

$$-\nabla \cdot \boldsymbol{q} = \rho \frac{De}{Dt}$$

Equation 4: Expression of energy balance (5)

Where:

- **q:** Heat flux vector.
- **ρ:** Density, which depends on temperature.
- **De/Dt:** Material derivative of the thermal energy density.
- **e:** Thermal energy density, defined as in Equation 5**.**

$$e = cT + \Delta h$$

Equation 5: Expression of thermal energy (5)

Where:

- **c:** Specific heat.
- **T:** Temperature, which depends on both space and time t.
- **Δh:** Latent heat, defined as Equation 6:

$$\Delta h = \begin{cases} L & T \geq T_l \\ \dfrac{T - T_s}{T_l - T_s} L & T_s < T < T_l \\ 0 & T \leq T_s \end{cases}$$

Equation 6: Expression of latent heat (5).

Where:

- **Ts and Tl:** Solidus and liquidus temperatures, respectively.
- **L:** Latent heat of fusion.

To solve the equation corresponding to Equation 1, it must determined how to obtain the value of the heat flux vector q, expressed as Equation 7:

$$\boldsymbol{q} = -\lambda \nabla T$$

Equation 7: Fourier's law (5).

Where:

- **λ:** Thermal conductivity.

The heat transfer problem, along with the initial and boundary conditions, is solved by considering Equation 8:

$$
\begin{aligned}
&T(x_1, x_2, x_3, 0) = T_{preheat}\ with\ (x_1, x_2, x_3) \in D \\
&T(x_1, x_2, x_3, 0) = T_r\ with\ (x_1, x_2, x_3) \notin D \\
&T(x_1, x_2, x_3, \infty) = T_r\ with\ (x_1, x_2, x_3) \notin D \\
&-\lambda \frac{\partial T}{\partial n}\Big|_{beam} = q - q_{rad} \\
&-\lambda \frac{\partial T}{\partial n}\Big|_{topsurface} = -q_{rad}
\end{aligned}
$$

Equation 8: Initial and boundary conditions of heat transfer (5).

Where:

- **D:** Interface between the substrate and the layer domains.
- **Tpreheat and Tr:** Preheating temperature and build chamber temperature, respectively.
- **qrad:** Heat loss by radiation, expressed as Equation 9:

$$q_{rad} = \varepsilon\sigma\left(T^4 - {T_r}^4\right)$$

Equation 9: Expression for radiation heat loss (5).

Where:

- **ε:** Emissivity.
- **σ:** Stefan-Boltzmann constant (5.67×10^{-8} W·m^{-2}·K^{-4}).

In Fig. 6, the boundary conditions of the model configuration can be observed (14).

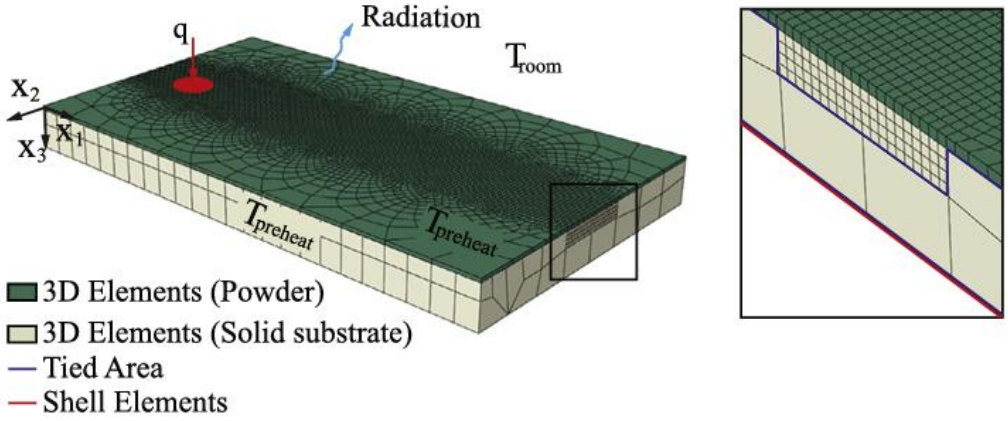

Fig. 6: FE model configuration, mesh strategy and boundary conditions.(14)

MATERIAL

The material used in this work is Ti6Al4V, which is a titanium alloy composed of approximately 5.5–6.75% aluminium and 3.5–4.5% vanadium, with the remainder being titanium (15)

The choice of this material for our model is due to its widespread use in EBM processes, thanks to its excellent mechanical properties, including high mechanical strength and hardness (16), its stability when working in a vacuum environment, as it maintains its properties under these conditions (17), and also its biocompatibility, which makes it very attractive for medical applications (18).

For our model, the following properties listed in Table 1 for Ti6Al4V will be used (14).

Material properties	
Density at 293 K [kg/mm^3]	3.93
Solidus temperature [K]	1873
Liquidus temperature [K]	1928
Latent heat [kJ/kg]	290
Average particle size [μm]	75
Porosity	0.32

Table 1: Material property list used in simulations(14).

METHODOLOGY

RESULTS EXTRACTION

As previously explained, with the simulations it is needed to extract the time at which the heat reaches the base of the powder, as well as how long it takes to reach the base of the powder considering the projection of the beam diameter. Specifically, a total of 20 simulations will be run varying the beam diameter and its power.

To do this, relying on the model previously developed in ABAQUS will be necessary.

To extract the moment when heat reaches the base of the powder, the “view cut” tool is first used to obtain a cross-sectional view of the model, allowing observation of how heat evolves in the interior region.

Once the cut is made, the “probe values” feature is employed to select the node where heat arrives first

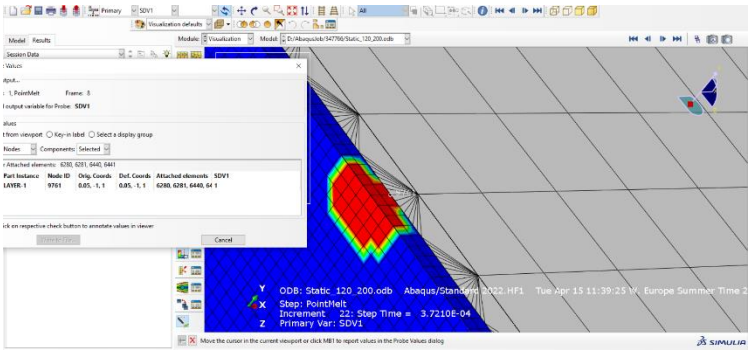

Fig. 7: Screenshot of the model in ABAQUS where the node selection is shown.

As can be seen in Fig. 7, this node is number 9761.

Once the node to study is identified, the ABAQUS tool “Create XY Data” is used. Here, the node to be analyzed is entered selecting select the variable SDV1, where the melting temperature of Ti6Al4V is defined. Once this is done, a data table will be generated, like the one in Fig. 8, showing time versus the point at which the material melts, taking the value 1 once melting has occurred. It is important to note that the first moment when the value reaches 1 is the instant that is needed to be recorded, as it represents the point when the heat reaches the layer of the powder.

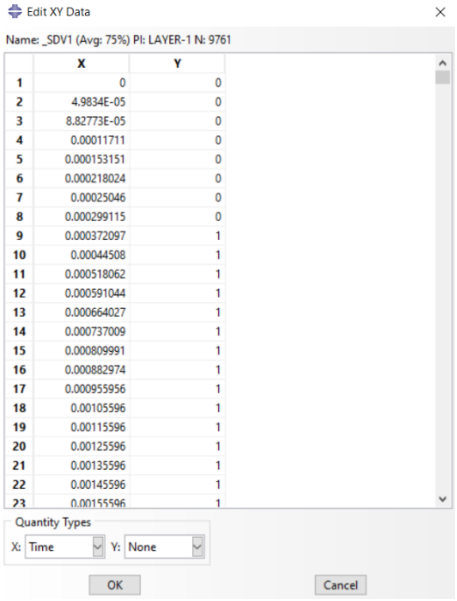

Fig. 8: Screenshot of ABAQUS of the XY data generated.

To obtain the value of the projected diameter, same process must be followed but selecting in “probe values” the projection of the beam diameter at the layer of the powder.

SIMULATIONS

For the first 4 simulations, a beam power value of 120 W is set, varying the beam diameter in each simulation.

Since this simulation uses the lowest beam power, is needed to set the beam working time to 0.1 seconds to ensure that our material melts up to the points needed.

This same process will be repeated for the 20 simulations in groups of 4, based on the beam power, obtaining the same data we are looking for in all of them.

During the simulation process, the beam operating time will be reduced because the higher the power, the shorter the times we are interested in. Therefore, the beam does not need to operate for as long to collect our data, which will save time and computational resources during the simulations.

Simulation 1

Beam Power: 120 (W)

Beam Diameter: 0,2 (mm)

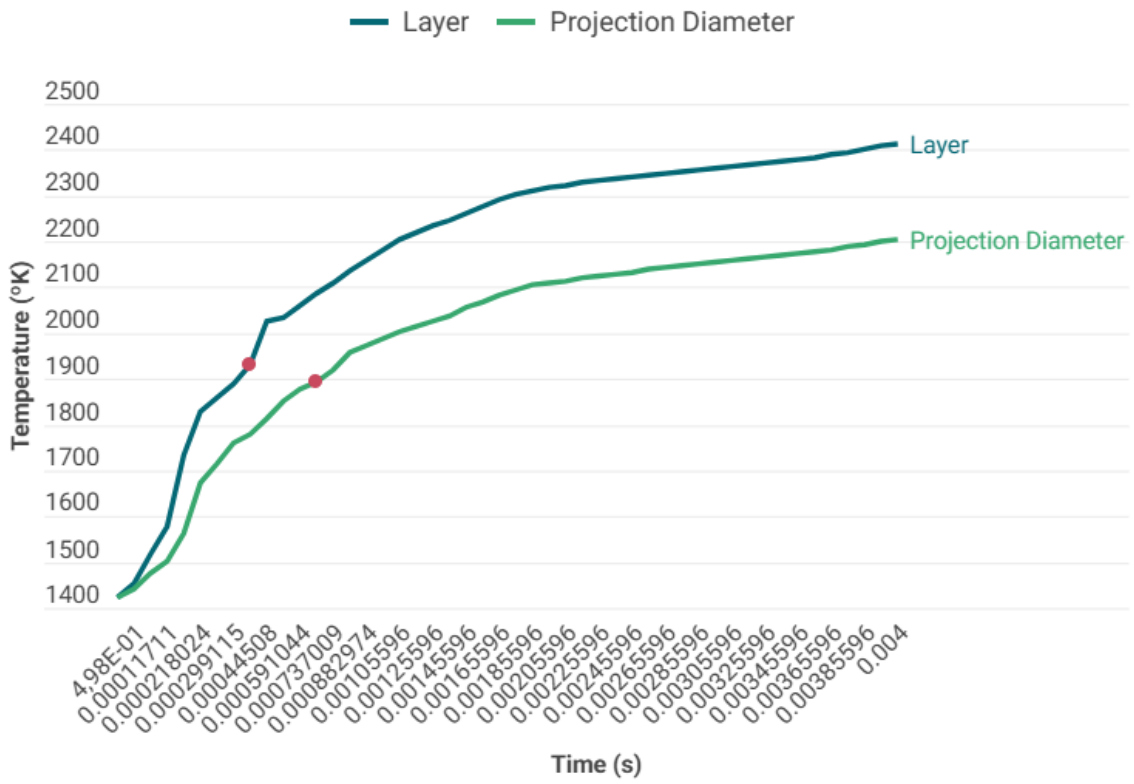

Fig. 9: Graph of the temperature of the powder layer as a function of the time for a beam configuration of 120W and 0.2mm in diameter.

With this simulation, temperature data at each moment for the points under study is obtained. Using these values, the following graph can be created plotting Temperature in Kelvin degrees versus time in seconds Fig. 9.

The blue line shows the temperature evolution at the central point where the beam strikes the layer of the powder.

The green line, on the other hand, shows how the temperature evolves at the projected point of the beam diameter, in this case 0.2 mm.

The red points indicate the moments when the material is fully melted; these values are recorded in Table 2.

Simulation Nr.	Beam Power (W)	Beam Diameter (mm)	Time Layer Powder (s)	Time Projection Diameter (s)
1	**120**	**0.2**	**0.000372097**	**0.000664027**

Table 2: Values of the moment when the material is fully melted for a beam configuration of 120W and 0.2mm in diameter.

This method of extracting the graph and then analyzing it to fill in the data for the table will be the same for all the simulations.

Simulation 2

Beam Power: 120 (W)

Beam Diameter: 0,3 (mm)

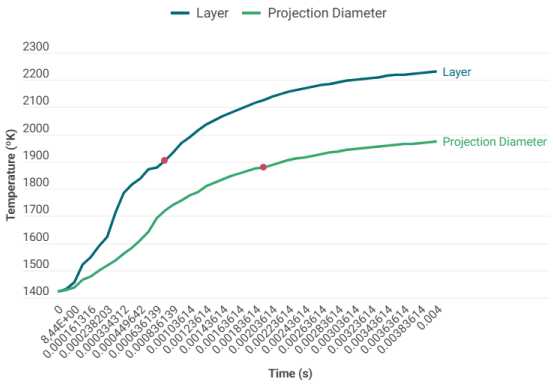

Fig. 11

Time Layer Powder (s)	Time Projection Diameter (s)
0.000736139	0.00193614

Table 3

Simulation 3

Beam Power: 120 (W)

Beam Diameter: 0,4 (mm)

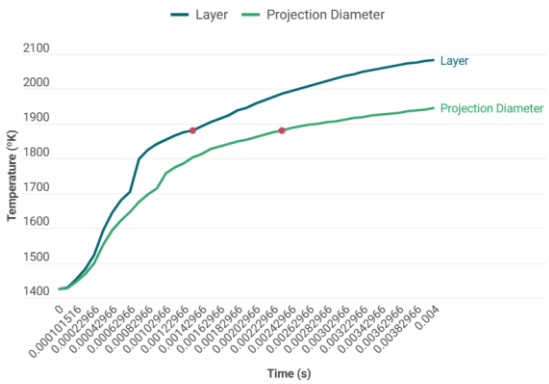

Fig. 10

Time Layer Powder (s)	Time Projection Diameter (s)
0.00132966	0.00232966

Table 4

Simulation 4

Beam Power: 120 (W)

Beam Diameter: 0,5 (mm)

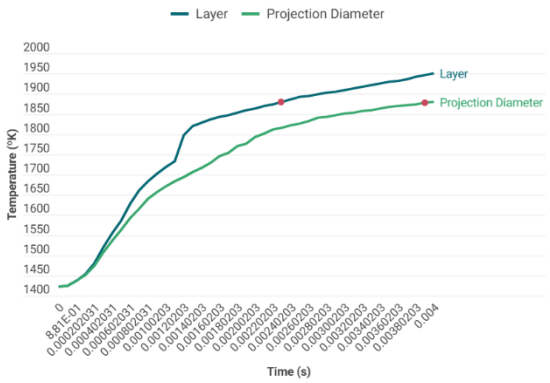

Fig. 12

Time Layer Powder (s)	Time Projection Diameter (s)
0.00230203	0.00390203

Table 5

Grouping all the results obtained regarding the times we were looking for with different diameters but the same power value Table 6,
we can generate the graph shown in Fig. 13 in order to have a more visual way to see the data, this graph plots time versus beam diameter for all cases in our simulations.

Simulation Nr.	Beam Power (W)	Beam Diameter (mm)	Time Layer Powder (s)	Time Projection Diameter (s)
1	120	0.2	0.000372097	0.000664027
2	120	0.3	0.000736139	0.00193614
3	120	0.4	0.00132966	0.00232966
4	120	0.5	0.00230203	0.00390203

Table 6: Values of the moment when the material is fully melted for a beam configuration of 120W for each diameter.

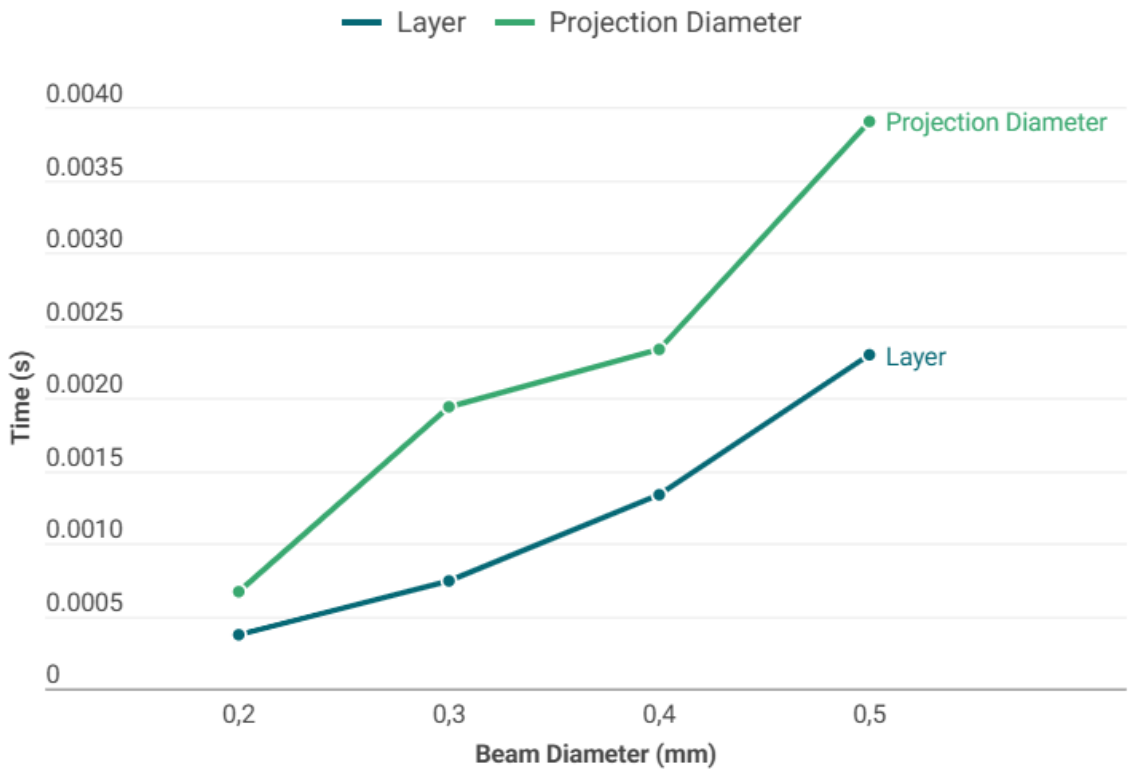

Fig. 13: Graph of the time for the heat to reach the powder layer as a function of the diameter for a beam configuration of 120W.

Simulation 5

Beam Power: 150 (W)

Beam Diameter: 0,2 (mm)

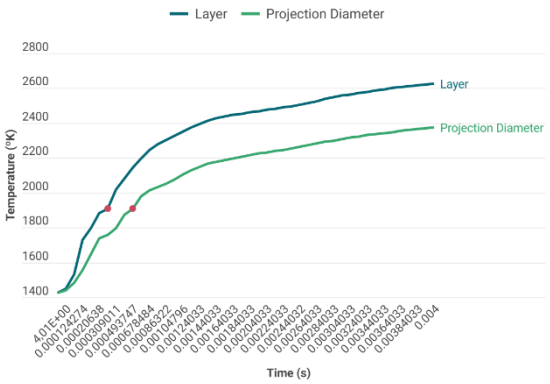

Fig. 17

Time Layer Powder (s)	Time Projection Diameter (s)
0.000247432	0.000493747

Table 10

Simulation 6

Beam Power: 150 (W)

Beam Diameter: 0,3 (mm)

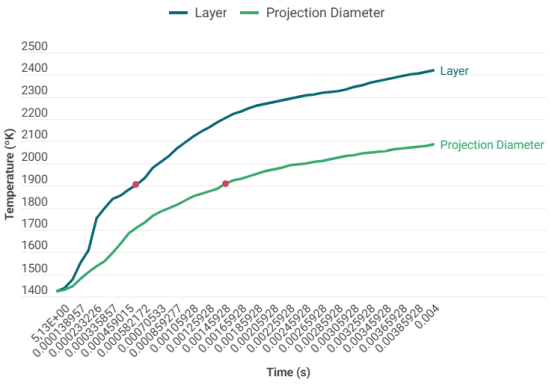

Fig. 16

Time Layer Powder (s)	Time Projection Diameter (s)
0.000520593	0.00145928

Table 9

Simulation 7

Beam Power: 150 (W)

Beam Diameter: 0,4 (mm)

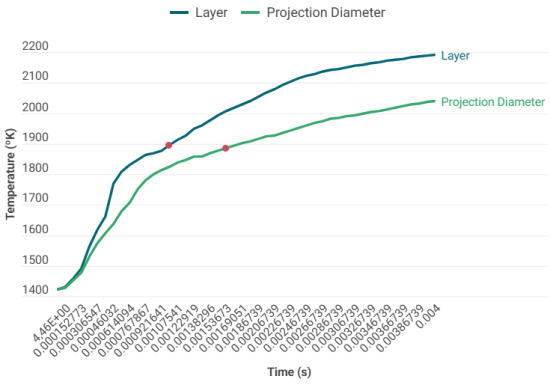

Fig. 15

Time Layer Powder (s)	Time Projection Diameter (s)
0.000998527	0.00153673

Table 8

Simulation 8

Beam Power: 150 (W)

Beam Diameter: 0,5 (mm)

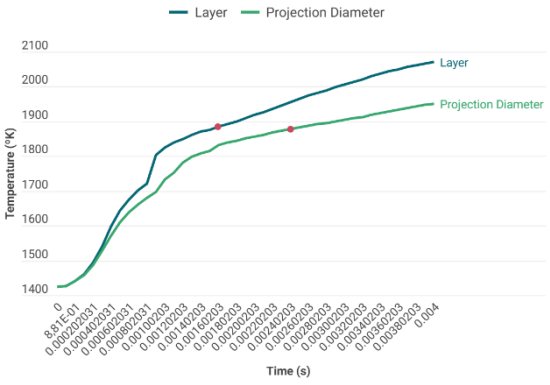

Fig. 14

Time Layer Powder (s)	Time Projection Diameter (s)
0.00160203	0.00240203

Table 7

Simulation Nr.	Beam Power (W)	Beam Diameter (mm)	Time Layer Powder (s)	Time Projection Diameter (s)
5	150	0.2	0.000247432	0.000493747
6	150	0.3	0.000520593	0.00145928
7	150	0.4	0.000998527	0.00153673
8	150	0.5	0.00160203	0.00240203

Table 11: Values of the moment when the material is fully melted for a beam configuration of 150W for each diameter.

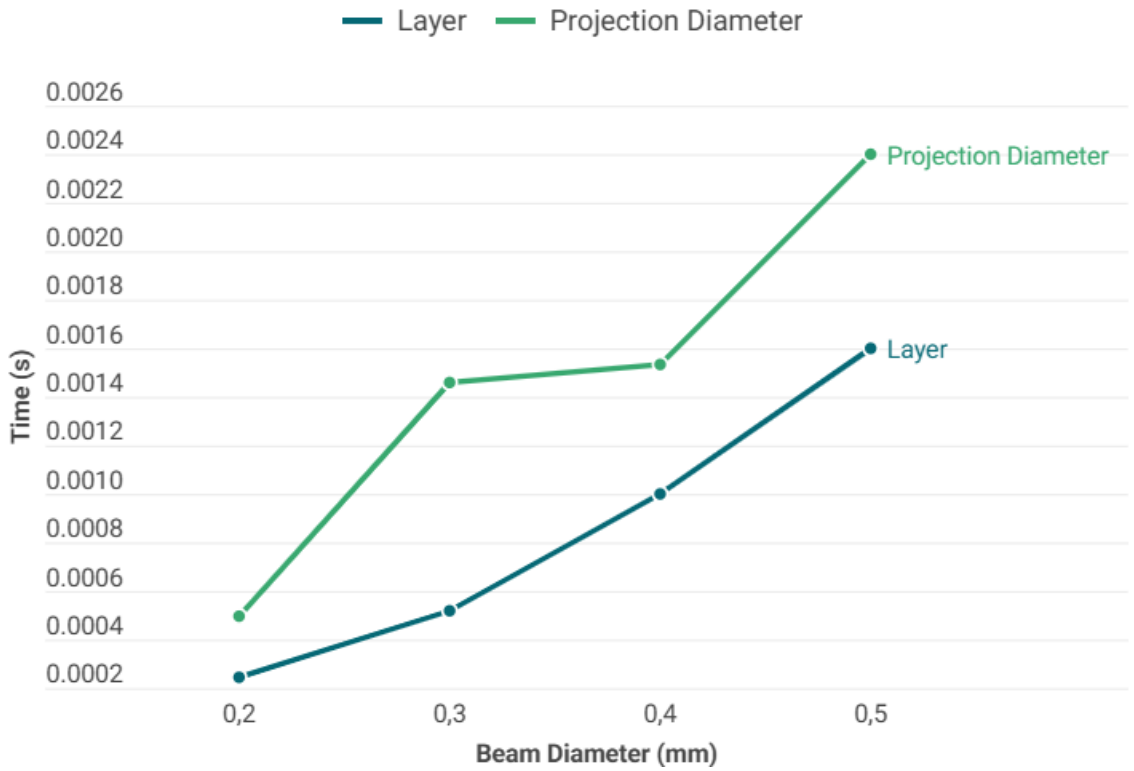

Fig. 18: Graph of the time for the heat to reach the powder layer as a function of the diameter for a beam configuration of 150W.

Simulation 9

Beam Power: 180 (W)

Beam Diameter: 0,2 (mm)

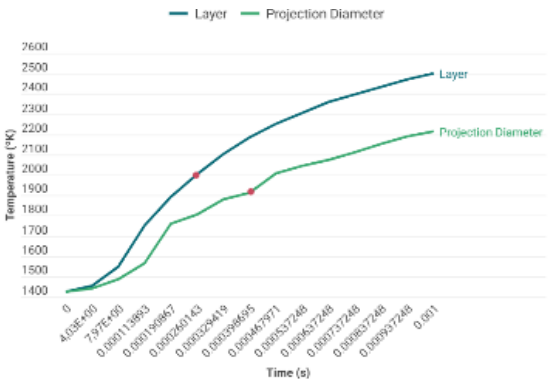

Fig. 20

Time Layer Powder (s)	Time Projection Diameter (s)
0.000260143	0.000398695

Table 13

Simulation 10

Beam Power: 180 (W)

Beam Diameter: 0,3 (mm)

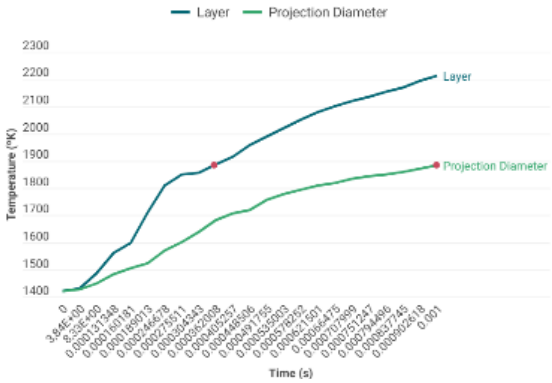

Fig. 21

Time Layer Powder (s)	Time Projection Diameter (s)
0.000362008	0.00103236

Table 12

Simulation 11

Beam Power: 180 (W)

Beam Diameter: 0,4 (mm)

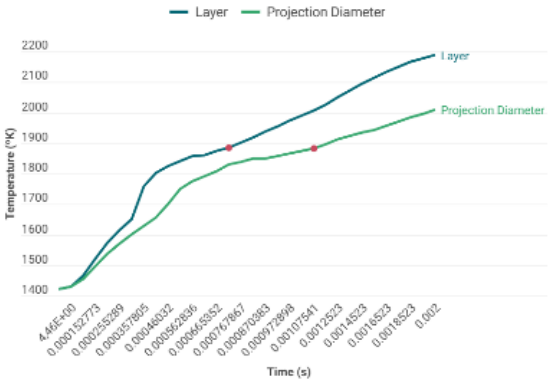

Fig. 22

Time Layer Powder (s)	Time Projection Diameter (s)
0.000716609	0.00107541

Table 15

Simulation 12

Beam Power: 180 (W)

Beam Diameter: 0,5 (mm)

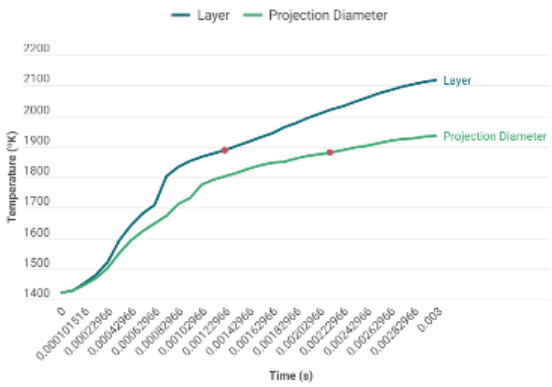

Fig. 19

Time Layer Powder (s)	Time Projection Diameter (s)
0.00122966	0.00212966

Table 14

Simulation Nr.	Beam Power (W)	Beam Diameter (mm)	Time Layer Powder (s)	Time Projection Diameter (s)
9	180	0.2	0.000260143	0.000398695
10	180	0.3	0.000362008	0.00103236
11	180	0.4	0.000716609	0.00107541
12	180	0.5	0.00122966	0.00212966

Table 16: Values of the moment when the material is fully melted for a beam configuration of 180W for each diameter.

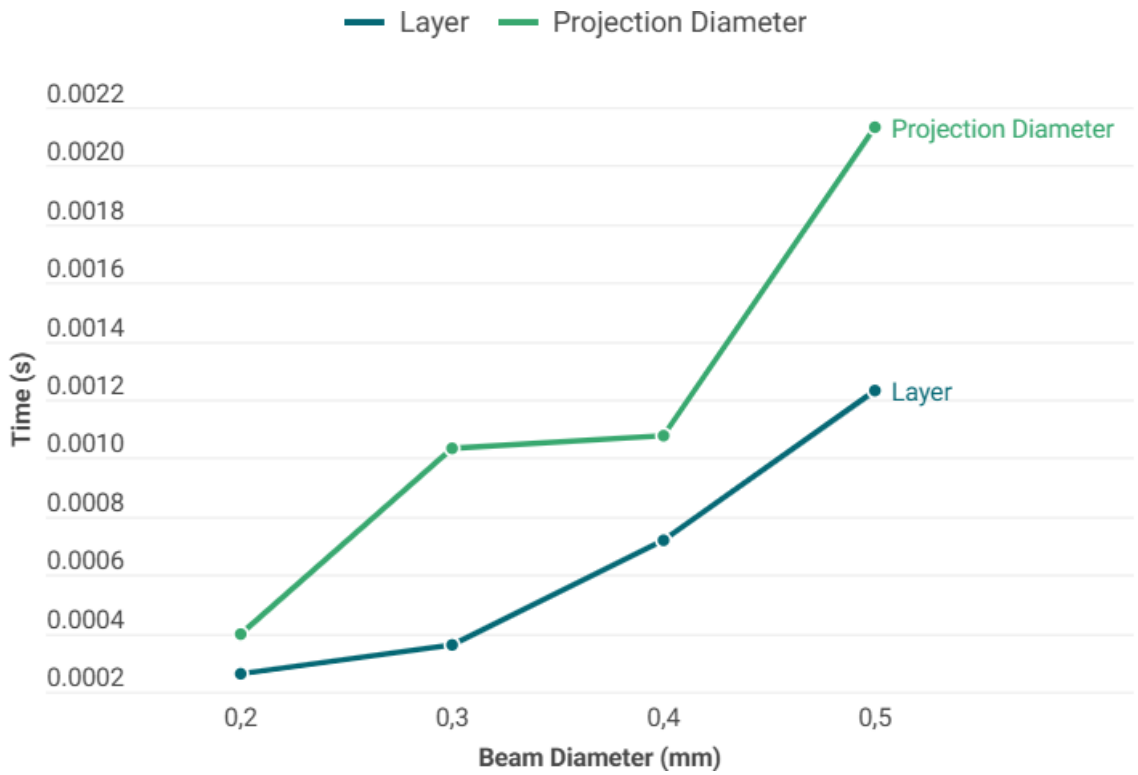

Fig. 23: Graph of the time for the heat to reach the powder layer as a function of the diameter for a beam configuration of 180W.

Simulation 13

Beam Power: 210 (W)

Beam Diameter: 0,2 (mm)

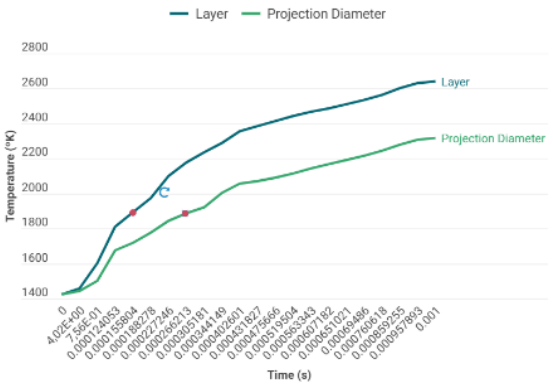

Fig. 27

Time Layer Powder (s)	Time Projection Diameter (s)
0.000155804	0.00026621

Table 20

Simulation 14

Beam Power: 210 (W)

Beam Diameter: 0,3 (mm)

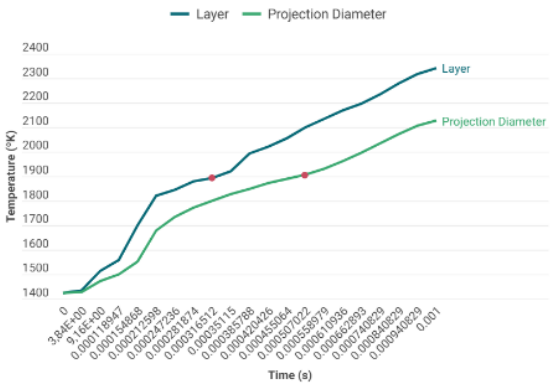

Fig. 26

Time Layer Powder (s)	Time Projection Diameter (s)
0.000316512	0.000507022

Table 17

Simulation 15

Beam Power: 210 (W)

Beam Diameter: 0,4 (mm)

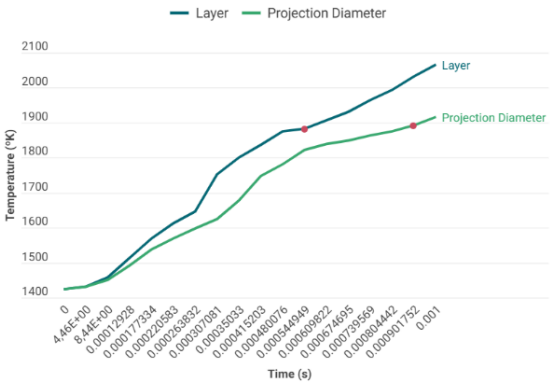

Fig. 25

Time Layer Powder (s)	Time Projection Diameter (s)
0.000544949	0.000901752

Table 18

Simulation 16

Beam Power: 210 (W)

Beam Diameter: 0,5 (mm)

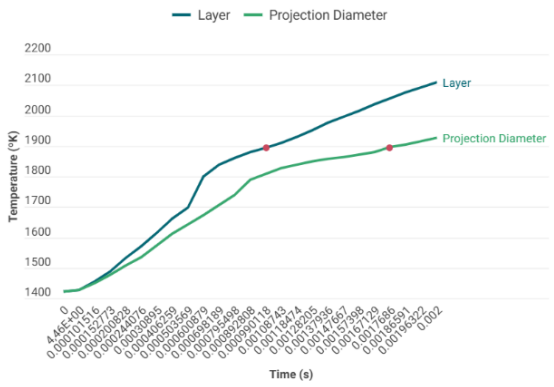

Fig. 24

Time Layer Powder (s)	Time Projection Diameter (s)
0.000990118	0.0017686

Table 19

Simulation Nr.	Beam Power (W)	Beam Diameter (mm)	Time Layer Powder (s)	Time Projection Diameter (s)
13	210	0.2	0.000155804	0.00026621
14	210	0.3	0.000316512	0.000507022
15	210	0.4	0.000544949	0.000901752
16	210	0.5	0.000990118	0.0017686

Table 21: Values of the moment when the material is fully melted for a beam configuration of 210W for each diameter.

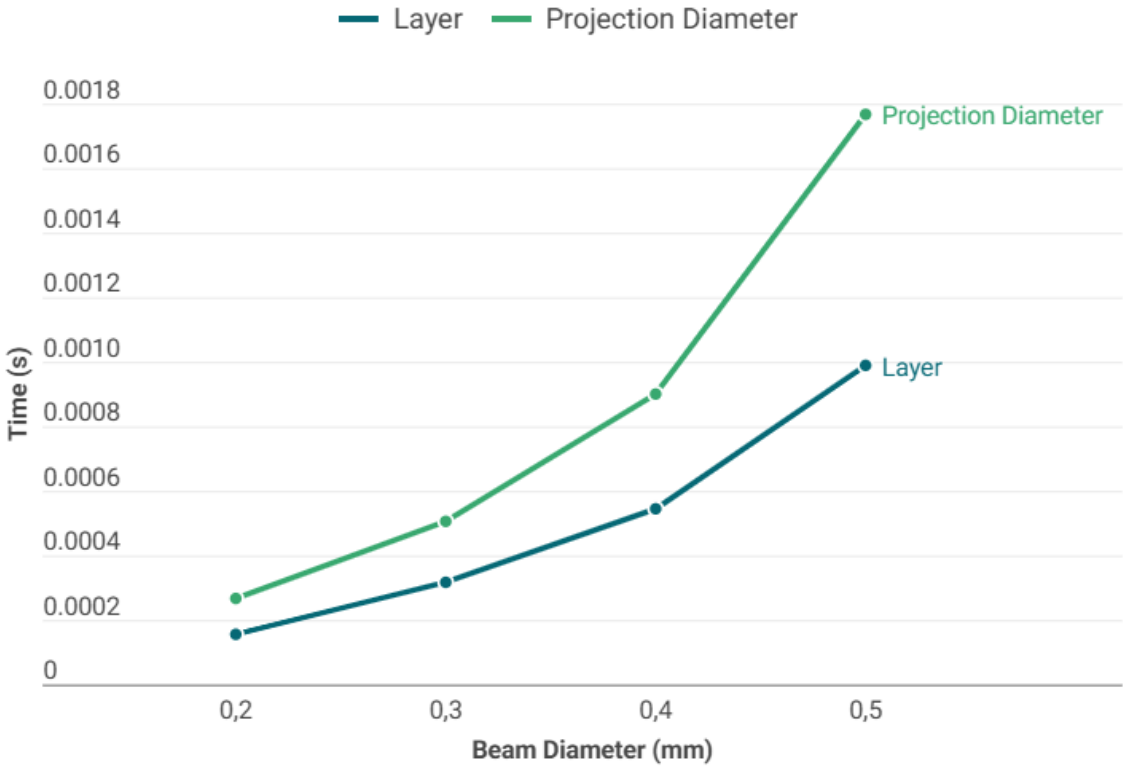

Fig. 28: Graph of the time for the heat to reach the powder layer as a function of the diameter for a beam configuration of 210W.

Simulation 17

Beam Power: 240 (W)

Beam Diameter: 0,2 (mm)

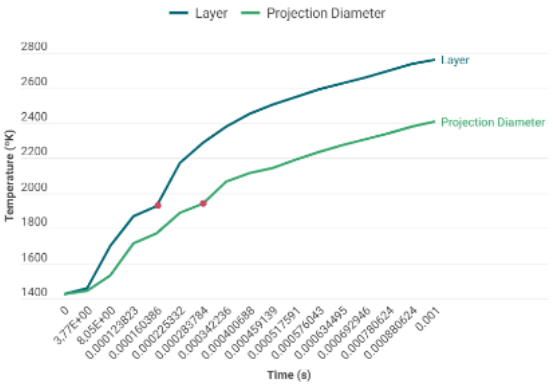

Fig. 32

Time Layer Powder (s)	Time Projection Diameter (s)
0.000160386	0.000283784

Table 25

Simulation 18

Beam Power: 240 (W)

Beam Diameter: 0,3 (mm)

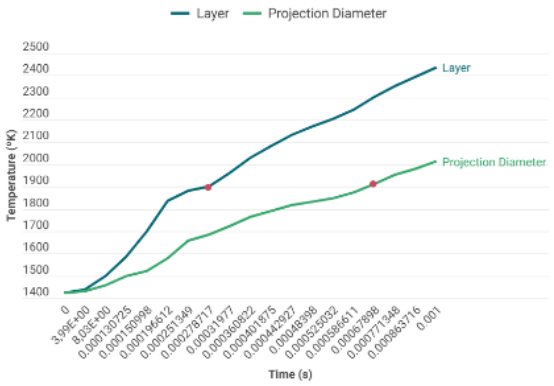

Fig. 29

Time Layer Powder (s)	Time Projection Diameter (s)
0.000278717	0.00067898

Table 22

Simulation 19

Beam Power: 240 (W)

Beam Diameter: 0,4 (mm)

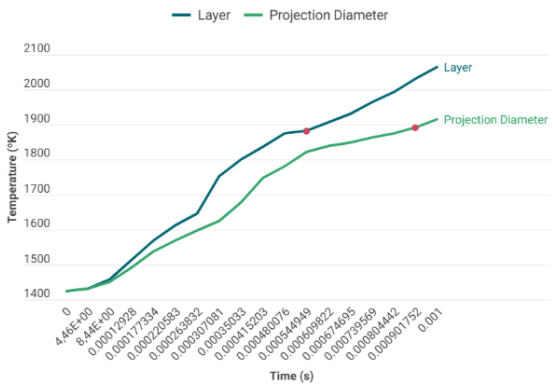

Fig. 30

Time Layer Powder (s)	Time Projection Diameter (s)
0.000552157	0.000725152

Table 23

Simulation 20

Beam Power: 240 (W)

Beam Diameter: 0,5 (mm)

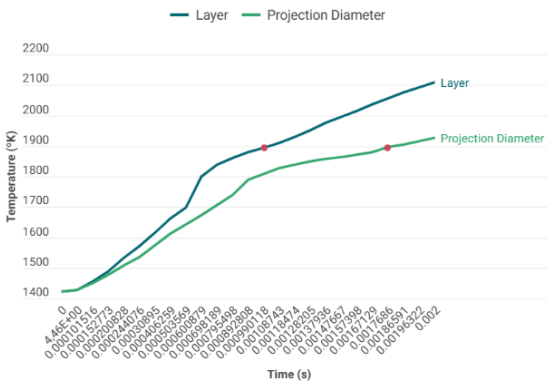

Fig. 31

Time Layer Powder (s)	Time Projection Diameter (s)
0.000844754	0.00138296

Table 24

Simulation Nr.	Beam Power (W)	Beam Diameter (mm)	Time Layer Powder (s)	Time Projection Diameter (s)
17	240	0.2	0.000160386	0.000283784
18	240	0.3	0.000278717	0.00067898
19	240	0.4	0.000552157	0.000725152
20	240	0.5	0.000844754	0.00138296

Table 26: Values of the moment when the material is fully melted for a beam configuration of 240W for each diameter.

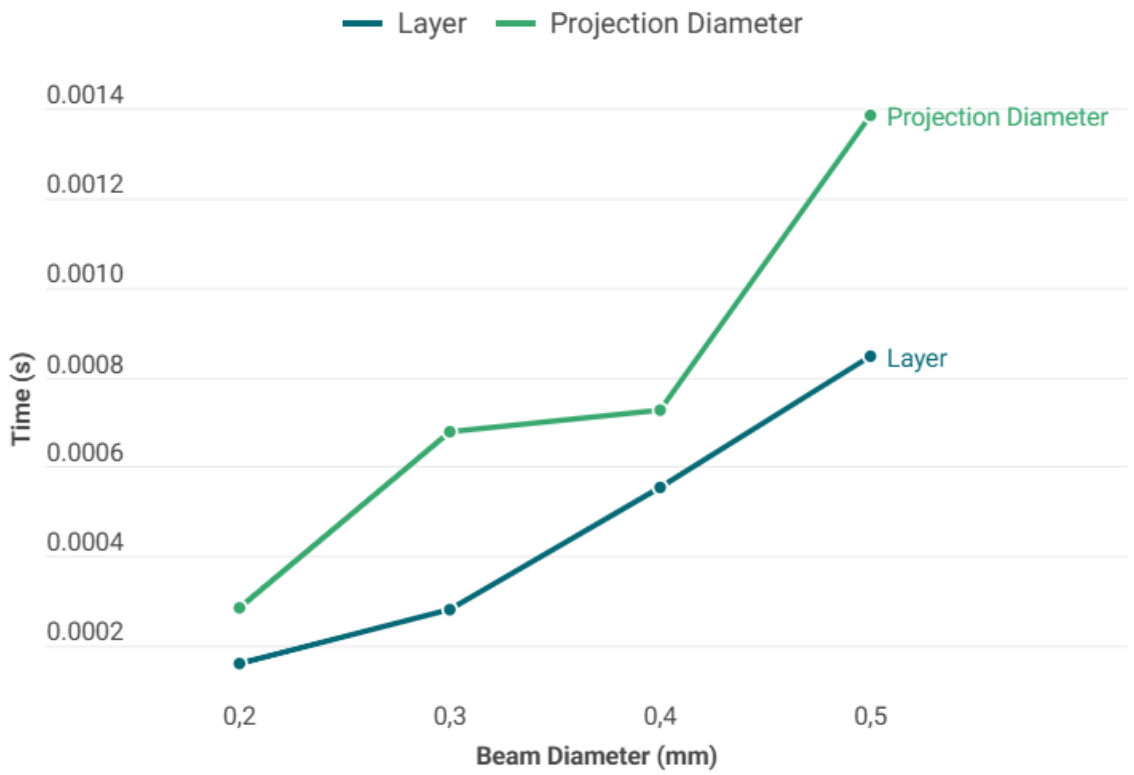

Fig. 33: Graph of the time for the heat to reach the powder layer as a function of the diameter for a beam configuration of 240W.

ANALYSIS OF THE RESULTS

Once all necessary data is obtained from the simulations, the study proceeds to analyze these data in order to draw conclusions.

To analyze them in a more visual way, two graphs are shown below.

The first graph, shown in Fig. 34, illustrates the time required for the heat to reach the powder layer for each power configuration as a function of the beam diameter. The second graph, in Fig. 35, presents a similar analysis, but in this case the time is for the heat to reach the projection of the beam diameter on the powder layer.

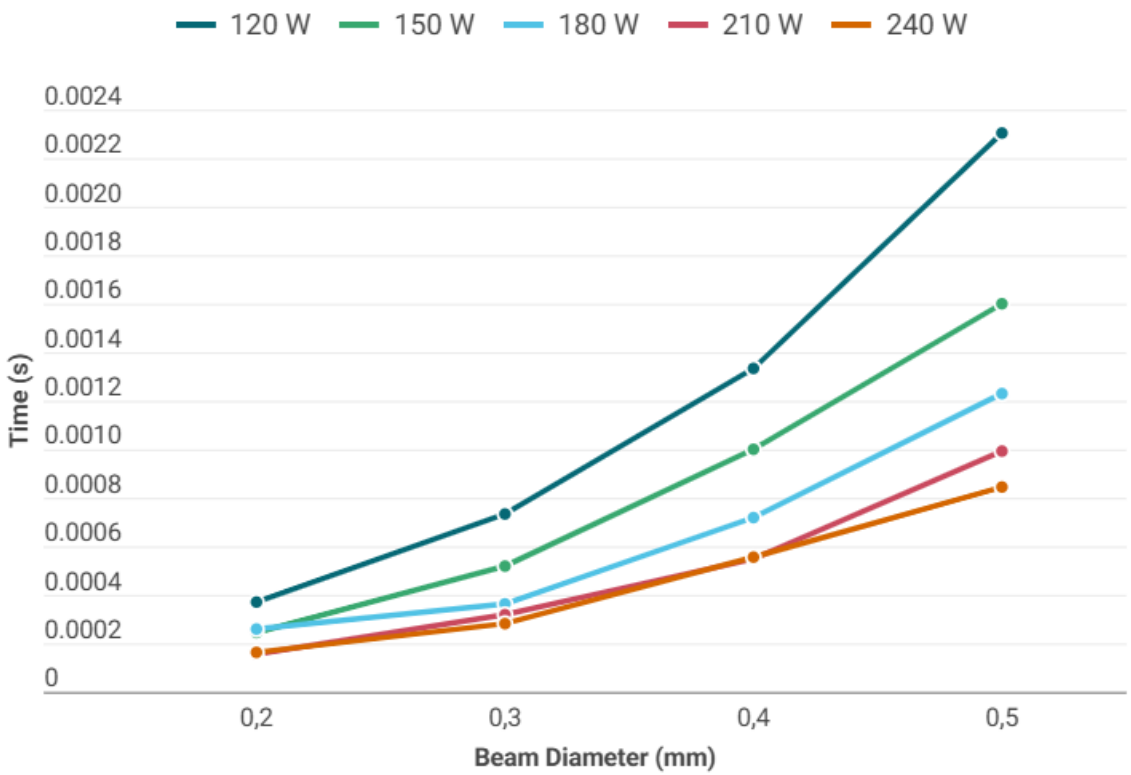

Fig. 34: Graph of the time for heat to reach the powder layer as a function of beam diameter for different beam power configurations.

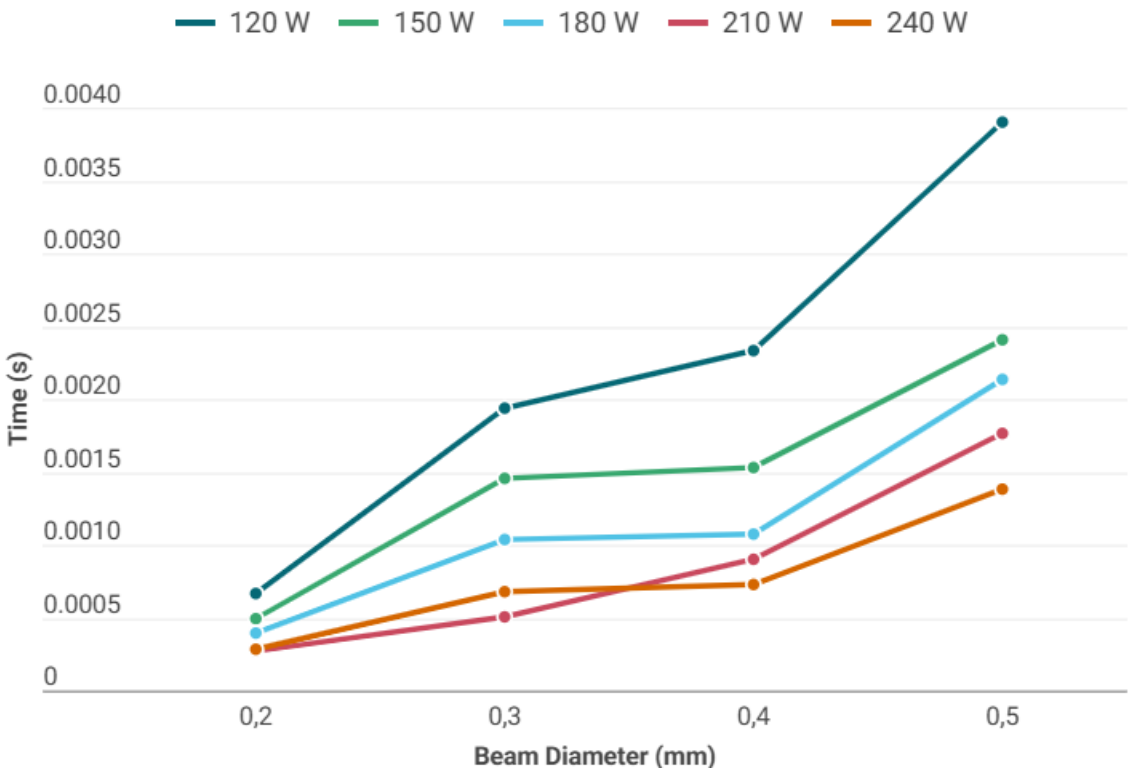

Fig. 35 Graph of the time for heat to reach the projection of the beam diameter on the powder layer as a function of beam diameter for different beam power configurations.

From Fig. 34 and Fig. 35, some conclusions can be drawn:

Trends:

- There is an inversely proportional relationship between beam power and the time it takes for the material to melt.
- The melting time increases exponentially as the beam diameter increases for all tested power levels.
- The difference in melting times between power levels becomes significantly more pronounced as the beam diameter increases.

Observing these trends, it can be generalized that the optimal choice in most situations is to work with a beam power of 210 W and a beam diameter between 0.2 mm and 0.3 mm.

This is because, despite the shorter melting times offered by using a power of 240 W, this can generate excessively high temperatures that may contribute to accelerated evaporation of the aluminium contained in the alloy, thereby reducing the mechanical strength of the final result (17). Since the difference in melting times compared to simulations performed at 210 W is not sufficiently significant (and in some cases even slower, such as at 0.3 mm when studying the time it takes to reach the projection of the diameter at the base), the risk involved is not

justified, in addition to the higher energy consumption when working at higher power.

Furthermore, a truly significant difference can be observed when comparing the times obtained at 210 W with those at 120 W, 150 W, and 180 W, so it can be almost automatically concluded that these lower power levels are not suitable when aiming for full process optimization.

In addition to studying power levels, the influence of beam diameters must also be considered carefully. A smaller beam will concentrate energy in a reduced area, offering more localized and precise melting of the metal powder. This allows for the manufacturing of parts with higher detail and more complex geometries.

These physical advantages are complemented by the fact that using a smaller diameter also results in shorter melting times, providing many benefits.

However, it should not be forgotten that with a smaller diameter, more points will be needed to complete each layer, which would translate into a significant increase in production time. Therefore, this must also be considered when choosing the beam diameter.

BIBLIOGRAPHY

1. Popov V V., Katz-Demyanetz A, Kovalevsky A, Biletskiy R, Strokin E, Garkun A, et al. Effect of the hatching strategies on mechanical properties and microstructure of SEBM manufactured Ti-6Al-4V specimens. Letters on Materials. 2018 Dec 1;8(4):468–72.

2. Gupta A, Bennett CJ, Sun W. The role of defects and characterisation of tensile behaviour of EBM Additive manufactured Ti-6Al-4V: An experimental study at elevated temperature. Eng Fail Anal [Internet]. 2021 Feb 1 [cited 2025 Sep 13];120:105115. Available from: https://www.sciencedirect.com/science/article/abs/pii/S1350630720316393

3. Raghavan S, Nai MLS, Wang P, Sin WJ, Li T, Wei J. Heat treatment of electron beam melted (EBM) Ti-6Al-4V: microstructure to mechanical property correlations. Rapid Prototyp J. 2018;24(4).

4. Balbás Calvo A, Espinosa M del M, Domínguez Somonte M. Últimos avances en la fabricación aditiva con materiales metálicos. Lámpsakos. 2018 Jan 16;(19):47–54.

5. Galati M, Iuliano L. A literature review of powder-based electron beam melting focusing on numerical simulations. Vol. 19, Additive Manufacturing. 2018.

6. Gokuldoss PK, Kolla S, Eckert J. Additive manufacturing processes: Selective laser melting, electron beam melting and binder jetting-selection guidelines. Vol. 10, Materials. 2017.

7. Mahale TR. Electron Beam Melting of Advanced Materials and Structures, mass customization, mass personalization. Vol. 91, NC State University. 2017.

8. Gaytan SM, Murr LE, Medina F, Martinez E, Lopez MI, Wicker RB. Advanced metal powder based manufacturing of complex components by electron beam melting. Materials Technology. 2009;24(3).

9. Heinl P, Rottmair A, Körner C, Singer RF. Cellular titanium by selective electron beam melting. Adv Eng Mater. 2007;9(5).

10. Murr LE, Gaytan SM. Electron Beam Melting. Comprehensive Materials Processing: Thirteen Volume Set [Internet]. 2014 Jan 1 [cited 2025 Jun 17];10:135–61. Available from: https://www.sciencedirect.com/science/article/pii/B9780080965321010049?via%3Dihub

11. Haveroth GA, Thore CJ, Ausas RF, Jakobsson S, Cuminato JA, Correa MR. Optimization of point-melting strategies for the Electron Beam Melting process. Finite Elements in Analysis and Design [Internet]. 2025 Jul 1 [cited 2025 Jun 17];249:104356. Available from: https://www.sciencedirect.com/science/article/pii/S0168874X25000459

12. EBM Point Melt Technology Technology [Internet]. Available from: www.colibriumadditive.com/resources

13. Galati M, Iuliano L, Salmi A, Atzeni E. Modelling energy source and powder properties for the development of a thermal FE model of the EBM additive manufacturing process. Addit Manuf. 2017;14.

14. Galati M, Snis A, Iuliano L. Experimental validation of a numerical thermal model of the EBM process for Ti6Al4V. Computers and Mathematics with Applications. 2019;78(7).

15. Arrazola PJ, Garay A, Iriarte LM, Armendia M, Marya S, Le Maître F. Machinability of titanium alloys (Ti6Al4V and Ti555.3). J Mater Process Technol [Internet]. 2009 Mar 1 [cited 2025 Jun 22];209(5):2223–30. Available from: https://www.sciencedirect.com/science/article/abs/pii/S0924013608004998

16. Gutiérrez Rodríguez LY, Jiménez Espinosa FA, Pertuz-Comas AD, González-Estrada OA, Díaz Rodríguez JG. Estudio de fatiga a bajos ciclos de la aleación Ti-6Al-4V obtenida por fusión de haz de electrones y su extensión a altos ciclos. Scientia et Technica. 2021 Sep 30;26(03):290–7.

17. Tamayo JA, Riascos M, Vargas CA, Baena LM. Additive manufacturing of Ti6Al4V alloy via electron beam melting for the development of implants for the biomedical industry. Vol. 7, Heliyon. Elsevier Ltd; 2021.

18. Preciado M, Bravo PM, Calaf J, Ballorca D. CARACTERIZACIÓN DE TI-6AL-4V FABRICADO MEDIANTE FUSIÓN POR HAZ DE ELECTRONES (EBM) POR LA TÉCNICA DE MINIATURA PUNZONADO.

19. Li JLZ, Alkahari MR, Rosli NAB, Hasan R, Sudin MN, Ramli FR. Review of wire arc additive manufacturing for 3d metal printing. International Journal of Automation Technology. 2019;13(3).